Design of a Small-Scale Supercritical Water Oxidation Reactor. Part II: Numerical Modeling and Validation

*Anmol L. Purohit[a], John A. Misquith[a], Brian R. Pinkard[a], Stuart J. Moore[a], John C. Kramlich[a], Per G. Reinhall[a], Igor V. Novosselov[a, b]**

[a] University of Washington, Mechanical Engineering Department, Seattle, WA 98195

[b] University of Washington, Institute for Nanoengineered Systems, Seattle, WA 98195

* Corresponding Author: ivn@uw.edu; +1 206 543-5248

Abstract

The experimental data from the laboratory-scale supercritical water oxidation reactor was leveraged to validate the CFD approach allowing for efficient and accurate modeling of the process. The reactor operating on ethanol as a pilot fuel was modeled using CFD with global oxidation mechanism. Fluid properties were determined using polynomial fit approximations, which yielded excellent agreement with NIST data over a range of temperatures at an isobaric pressure of 25 MPa. The model predicts the fluid temperature within 30°C of measured values for different inlet fuel concentrations. The ethanol decomposition of ~99% occurs within 20% of the reactor length at T~600 °C. The analysis of Damkohler (*Da*) and Reynolds (*Re*) numbers shows that the reactor operates in a distributed reaction region, owing to the excellent combustion stability of the inverted gravity reactor configuration. The modeling approach can aid the design of future more complex SCWO reactors and process optimization.

Keywords: Supercritical Water, Oxidation, Computational Fluid Dynamics, SCWO, Toxic Waste Destruction

1. Introduction

The thermophysical properties of supercritical water (SCW) are well-suited for destruction of organic waste such as sewage sludge,[1-3] industrial effluents,[4-6] and chemical warfare agents.[7-9] Along the 25 MPa isobar, the dielectric constant of water drops from 79.8 at 25 °C to 1.99 at 425 °C as it transitions across the critical point (22.1 MPa, 374 °C), creating a dense non-polar reaction environment where organic compounds are readily are miscible in supercritical mater. The absence of surface tension results in a single-phase reaction medium,[10-12] similar to gas-phase volumetric reactions in combustion. Supercritical water oxidation (SCWO) is effective at converting the organic compounds to CO_2, H_2O, and N_2, while heteroatoms such as Cl, S, F, and P, that can be present in the feedstock, are converted to acids and salts. In the treatment of toxic organic waste SCWO has an advantage over incineration in waste because of the lower operating temperatures in SCWO, which inhibits the production of NO_x, SO_2, and particulate matter (PM). One of the main challenges in adoption is related to thermal management of the reactor; others include material limits, corrosion,[13] and wall scaling.[14-16] The insights into the reactor operation, such as temperature profiles in fluid and structural features (wall, liner, injectors, etc.), species distribution, and location of liquid/supercritical phase transition, are essential in the reactor design and optimization of its operational parameters. The challenges related to reactor modeling include (i) difficulties in modeling mixture properties around the transition point, (ii) lack of high-quality experimental data that includes detail product yields, residence time and temperature measurements, (iii) lack of detailed chemical mechanisms for the oxidation of more complex organic compounds in supercritical water.

Most previous SCWO modeling efforts have been focused on single-phase reactor design. However, to manage the fate of ionic compounds, it may be necessary to maintain a subcritical region. Thus, it is essential to accurately capture the change in thermophysical properties across the critical point. The thermochemical properties mainly, specific heat capacity (C_p), thermal conductivity (k), viscosity (μ), density (ρ), and dielectric constant (ε) change rapidly and drastically across the critical point. These properties are hard to measure and are available only for a limited number of compounds. Fortunately, properties of the most abundant compounds in the SCWO process, such as H_2O, CO_2, N_2, and O_2 are available from the NIST database.[17] Properties of some fuels (e.g., ethanol) and the intermediates (e.g., formic acid) are available for a limited range as these compounds undergo decomposition in the high-temperature, high-pressure environment.[18-23] Most properties can be modeled using a piecewise polynomial fit based on the NIST data. For accurate prediction of the transition point, an accurate description of water properties presents the greatest challenge. The spike in C_p around the transition point can be readily described using look-up tables; this strategy is numerically inefficient.

Several researchers have reported kinetic rates for SCWO of ethanol[21, 24-27] and methanol.[28-30] Rice and Croisset[26] first provided a detailed mechanism for ethanol oxidation in supercritical water which was later updated by Hong et al.[27] based on their experimental and modeling analysis. Simulating a detailed kinetic mechanism coupled with other CFD governing equations is computationally expensive. Global kinetics are more efficient to analyze the energy release and the major species formation in the reactor. Helling and Tester[24] proposed a three step oxidation mechanism for ethanol. Later, Schanzenbächer et al.[25] further reduced the 3 step oxidation kinetics by Helling and Tester to single step kinetics. By improving the experimental setup and

measurements, Schanzenbächer et al.[25] was able to account for induction time due to mixing which resulted in an improved estimate of the activation energy for SCWO of ethanol as 163 kJ mol^{-1}. Kinetic rates have also been proposed for more recalcitrant SCWO feedstocks, such as CWA surrogates. For example, DMMP (surrogate for GB and GD) decomposes relatively fast via hydrolysis[31] yielding a recalcitrant intermediate product, methylphosphonic acid (MPA).[8, 32, 33] Destruction of MPA requires high temperature (T>600°C) and high residence time (τ > 10 s); reported reaction kinetics allow for integration of multiple mechanistic models within a single reactor domain. Insights from CFD modeling such as temperature and exposure time in a continuous flow reactor can aid the reactor design and optimization of operating conditions for a practical system. Most kinetic rate studies of SCWO reactions have been conducted in tubular reactors assumed to operate in a plug-flow regime (PFR) where hydrodynamic effects are negligible; in contrast, practical SCWO systems would have influences of turbulent mixing, buoyancy, and fluid dynamics effects. Provisions for reactor start-up, control of wall and fluid temperatures are essential for the safe operation of the reactor.

Several CFD studies addressed specific aspects of the SCWO phenomena and to validate experimental results.[34-36] Segal et al.[37] proposed a mathematical model for a jet breakup in subcritical and supercritical medium and the effect of the critical phase transition on surface tension. Zhang et al.[38] evaluated the mixing enhancement of jets in a supercritical environment as a function of jet velocity and temperature. Moussière et al.[39, 40] studied the effect of turbulence on oxidation rate and heat release. Huo et al.[41] studied the relation between heat release, pressure, and strain rate in counterflow flame. Lacaze and Oefelein[42] investigated flame structure in non-premixed supercritical combustion as a function of pressure and temperature. Though some papers

reported SCWO reactor modeling,[35, 39, 43, 44] a parametric comparison against a comprehensive set of data has not been presented in the literature.

Inverted gravity (downflow) configuration presents a possible solution for achieving the long residence time requirements for the destruction of refractive species. In the stratified state, the supercritical zone is located near the fuel injection port, while subcritical liquid water can pool at the bottom, not affecting the ignition and reaction stability. Downflow reactor designs have been explored in gaseous combustion systems and SCWO reactors. Buoyancy stabilized inverted gravity flames reactors exhibit excellent stability and high residence times (τ_{res}) compared to upright flame configurations. The residence time is controlled by altering the balance of the convective and buoyant terms, leading to the onset of large-scale recirculating patterns in the reactor.[45] The long residence time has been utilized for synthesis nanoparticles[46] and in studies of the particle formation and aggregation mechanisms.[47-49] The temperature control is typically accomplished by diluting the fuel stream. Hydrothermal flame reactors are operated in the upright configuration;[50 51] these provide high flame temperatures but very low residence times and small reaction region. Most SCWO reactors utilize the downflow arrangement[52-55] to achieve long residence times and uniform temperature profiles needed for hazardous waste destruction.

In the downflow configuration, the interplay between the characteristic mixing and chemical times is significantly different than in the upright flame; most importantly, the chemistry can be stabilized at the low temperatures. These differences are reflected in ignition and flame stability. In this work, we do not analyze the ignition characteristics, and we limit the analysis to steady-state operation at various fuel dilution conditions. The temperature is controlled by the fuel dilution, and reaction stability is examined. The approach is analogous to work related to

combustor lean blowout (LBO). Glassman related LBO to a ratio of the residence time and chemical kinetic time scale, also known as the Damkohler (*Da*) number. The chemical reaction time scale (τ_{chem}) is based on the Arrhenius chemical kinetic rate and is independent of the geometry length scales. In the perfectly stirred reactor (PSR) limit, the residence time in the combustion system must be greater than the chemical reaction time to sustain combustion.[56] An alternative definition of *Da* is a ratio of turbulent time scale to the characteristic chemical time scale $Da = \tau_{turb}/\tau_{chem}$, which is often used to study turbulent premixed flames.[57] The transient behavior of the flames, when stabilized by a recirculating flow, can significantly affect the LBO.[58] Various laboratory jet-stirred reactors (JSR) have been used to study LBO as the system approaches the threshold values fuel air-fuel equivalence ratios or reactor loadings.[59-62] With a decrease in residence time and an increase in the chemical times, the reactor approaches uniform temperature and species field distribution; this condition is known as distributed reaction region and can be characterized by *Da* and turbulent Reynolds (*Re*) numbers known and Klimov-Williams criterion.[63] These conditions are associated with an elevated level of intermediate species (e.g., OH, CO, CH, CH_3, HCO) associated with incomplete combustion leading to LBO. Detailed numerical modeling of these reacting systems is challenging due to the complexity of the interaction between turbulence and chemistry. The Reynolds-averaged Navier-Stokes (RANS) model is often used in modeling industrial combustors due to its low computational cost.[64] To incorporate combustion chemistry in flow simulations, Magnussen et al. proposed an eddy dissipation concept (EDC) model,[65-67] which was used to model turbulent combustion, including laboratory reactors [68, 69] and industrial burners. Modeling of laboratory system with reduced and skeletal chemical kinetics mechanism have shown promising results and identified a shift in flame location, quenching in chain branching reactions and presence of high concentrations of OH

radicals approaching LBO.[59, 70, 71] Guan et al. reported that the *Da* in the stabilization zone could be considered as the critical blowout parameter,[72] the stabilization zone $Da < 0.2$ to 0.3 was associated with LBO of toroidal JSR, however even at these conditions, the reactor had significant gradients in the species and temperature profiles. With the high turbulent *Re* in the JSR, the distributed reaction region was not achieved. In buoyancy stabilized SCWO reactor, the *Re* are significantly lower, so even a relatively high *Da* number may yield a distributed reaction region.

In this study, we perform CFD simulations of a laboratory SCWO reactor operated on ethanol as a fuel and H_2O_2 oxidant;[73] the data were taken for variable fuel dilutions for three locations within the reactor and several reactor wall locations. The supercritical water properties were model using polynomial fits of NIST data to speed up the computational time. The approach was validated against the experimental data for non-reactive flow and showed excellent agreement in the transition from supercritical to a subcritical fluid. The heat transfer through the reactor walls was modeled explicitly to match the heat loss from the reactor. Then the SCWO process was modeled using a single-step chemical kinetic mechanism[25] with finite rate and EDC approaches. The insight from the CFD can be used for future reactor optimization.

2. Model Development

2.1 ***CFD Model***

The CFD domain is designed to correspond with the dimensions of the SCWO reactor described in the adjacent paper.[73] The computational domain comprises a fluid mesh representing the reactor zone and a solid mesh to simulate the heat transfer through the walls of the reactor and insulation, as shown in Figure 1. The fluid domain consists of two coaxial, inlet tubes representing

the fuel and the oxidant line, respectively. Pipe thickness is also considered in the model to account for any heat transfer in the inlet tubes before the fluids enter the bulk of the domain. A composite slab approach is taken to model the walls and insulation around the reactor. Each solid is modeled to ensure accurate heat transfer. The solid wall zone layers consist of the reactor wall, a copper coil (which was in place to allow for active cooling of the reactor walls if needed but was not used), and two insulation layers: ceramic and glass fiber. The overall computational domain is constructed as a two-dimensional, axisymmetric model. The inner diameters of the fuel and oxidant lines are 0.6 mm and 3.9 mm, respectively. The reactor length measured from the tip of the fuel nozzle to the bottom is 355 mm. A titanium liner inserted in the reactor body has an inner diameter of 25mm; the heat transfer through the liner was not modeled due to its relatively small thickness compared with the outer reactor wall (0.89 mm vs. 6.35 mm). 2D axisymmetric mesh contained quad cells, and after performing mesh independence analysis, it had ~400,000 elements. The elements near the nozzle are ~ 0.1 mm; the rest of the elements, including the solid mesh, are ~ 0.8 mm.

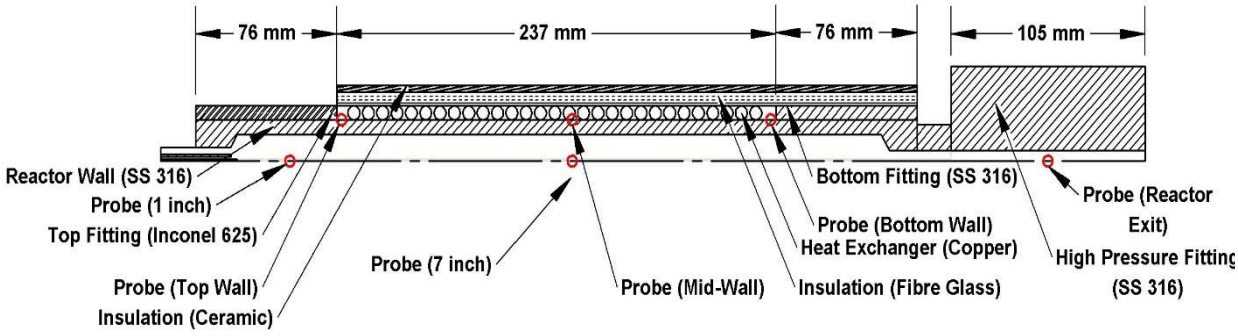

Figure 1. Schematic of the reactor used to make the CFD domain. The domain is solved as an axisymmetric problem.

Table 1 shows the material properties of the reactor wall and insulation. A mixed heat flux boundary condition is applied at surfaces exposed to ambient air accounts for convection and

radiation to simulate heat transfer. A heat transfer coefficient (h) of 15 W m^{-1} K^{-1} (assuming T_∞=27 °C) is used at the walls and insulation to account for natural convection of the surrounding air.

Table 1. The material properties of the walls and insulation material used in the experiments. These values are used in the CFD to simulate the heat loss from the reactor.

Material Name	Density (kg m^{-3})	Specific Heat (J $kg^{-1}K^{-1}$)	Thermal Conductivity (W $m^{-1}K^{-1}$)
Inconel 625	8440	520	15.5
Stainless Steel 316 (SS316)	8030	500	17.0
Copper	8978	381	258.0
Insulation - Ceramic	128	1130	0.13
Insulation - Fiberglass	140	870	1.2

2.2 Governing Equations and Models

The CFD solves Navier-Stokes equations (NSE) as a conservation of mass, momentum. Solving for energy conservation and transport is required when considering reacting flows. Conservation of mass is written as:

$$\frac{\partial \rho}{\partial t} + \nabla \cdot \rho \mathbf{u} = 0, \tag{1}$$

where

$$\nabla \cdot \rho \mathbf{u} = \frac{\partial \rho \mathrm{u}_x}{\partial \mathrm{x}} + \frac{\partial \rho \mathrm{u}_x}{\partial \mathrm{x}} + \frac{\rho \mathrm{u}_r}{r}, \tag{2}$$

ρ is the fluid density and $\mathbf{u}$ is the velocity vector in the x and radial direction. Species transport is required for solving chemical reactions, for species Y_i:

$$\frac{\partial \rho Y_i}{\partial t} + \nabla \cdot (\rho \mathbf{u} Y_i) = -\nabla \cdot \vec{J_i} + R_i + S_i, \tag{3}$$

Where J_i is the diffusion flux of species i, R_i is the production of i^{th} species and S_i is a user defined source or addition of species i from a dispersed phase. Momentum conservation is written as:

$$\frac{\partial \rho \mathbf{u}}{\partial t} + \frac{\nabla . \rho \mathbf{u}\mathbf{u}}{r} = -\nabla p + \frac{\nabla . \tau}{r} + \rho \mathbf{g}, \tag{4}$$

where

$$\tau = \mu \left(\nabla \mathbf{u} + \nabla \mathbf{u}^T - \frac{2}{3} (\nabla \cdot \mathbf{u}) \mathbf{I} \right), \tag{5}$$

and p is the hydrodynamic pressure, μ the dynamic viscosity, and $\boldsymbol{g}$ the gravitational vector. The energy (E) is balanced using the equation:

$$\frac{\partial}{\partial t}(\rho E) + \nabla \cdot \left(\mathbf{u}(\rho E + p) \right) = \nabla \cdot \left(k_{eff} \nabla T - \sum_i h_i \vec{J}_i + \overline{\overline{\tau}_{eff}} \cdot \mathbf{u} \right) + S_h, \tag{6}$$

where k_{eff} is the effective conductivity $k + k_t$, (k_t is the turbulent thermal conductivity), S_h is the source of energy from chemical reactions. The k-ω model shown good agreement with experimental data over a range of nozzle shapes and pressures in previous simulations[40, 74, 75] and it is used in this work.

The boundary and operating are assigned as below. The fuel and oxidant lines are defined as mass flow inlets, and the exit is modeled as a pressure outlet. The total domain pressure is held constant at 25 MPa. The ratio of Grashof (*Gr*) and the square of *Re* number for our modeled conditions vary in the range of 149 to 1680, indicating a strong effect of natural convection within the reactor.[76] Gravity is assigned in the positive x-direction to include buoyancy effects. A coupled pressure-velocity scheme is used, and second-order discretization is applied for energy, momentum, turbulence, and pressure. The residual imbalance of converged solutions was less than 1E-05 for all variables.

2.3 *Polynomial Fits to Model Thermal Properties*

Polynomial fits are generated using NIST data to model ρ, C_P, k, and μ. A temperature range (250 to 1000 °C) defining our experiments' temperature bounds is loaded into the NIST RERFPROP software[17] as a function of temperature for a constant pressure of 25 MPa. To increase the accuracy of prediction by the fits, piecewise polynomials are generated for all properties. The Fluent solver has a limitation of using up to 3 piecewise polynomials for a particular property that is not sufficient to accurately capture C_p of water that has steep transition across the critical region. To capture the shape, we used a multi-temperature range polynomial implemented through a user-defined function (UDF). The polynomial fit for a specified temperature range is given as:

$$C_p = a + b * T + c * T^2 + d * T^3 + \cdots, \tag{7}$$

where, a, b, c and d are respective coefficients fitted to capture the right property values. Similar to Equation 7, polynomial fits for other properties are also determined. The values for the coefficients to model properties of different species is given in Table 2.

Table 2. Coefficients of the polynomial fit for different temperature range to model thermophysical properties for species at 25 MPa

C_p for H_2O							
Temperature range (K)	**a**	**b**	**c**	**d**	**e**	**f**	**g**
523-600	68469.7	-241.062	0.228273	-	-	-	-
600-630	605982	-2003.34	1.67297	-		-	-
630-650	8919020	-28193.5	22.3004	-	-	-	-
650-658	334752000	-1029650	791.808	-	-	-	-
658-660	-101330000	322934	-256.559	-	-	-	-
660-668	260837000	-781911	586.025	-	-	-	-
668-700	4940260	-14135	10.125	-	-	-	-
700-850	1180040	-4365.4	5.40459	-0.00223261	-	-	-
>850	2800	-	-	-	-	-	-
ρ for H_2O							
300-670	-62867.91	919.1584	-5.426184	0.01683334	-2.895875e-05	2.61968e-08	-9.74180e-12
670-1200	23760.3	-119.0825	0.2457679	-0.0002663614	1.598095e-07	-5.03411e-11	6.50853e-15
k for H_2O							

523-659	81.5617	-0.399811	0.000660346	-3.65142e-07	-	-	-
659-778	3415.61	-18.7813	0.0387039	-3.54258e-05	1.21514e-08	-	-
778-1270	0.0540016	2.56843e-05	4.25319e-08	-	-	-	-
μ for H_2O							
523-673	-0.00227883	8.1606e-06	-7.03606e-09	-	-	-	-
673-1000	2.386938e-06	3.796289e-08	-8.081617e-13	-	-	-	-
C_p for O_2							
300-1100	2809.3391	-9.5365138	0.01885179	-1.60223E-05	5.00288E-09	-	-
ρ for O_2							
300-1100	1430.2325	-7.3221864	0.017634341	-2.2069E-05	1.39053E-08	-	-
k for O_2							
300-1100	0.026978374	3.82355E-05	9.61152E-09	-	-	-	-
μ for O_2							
300-1100	1.84787E-05	3.29596E-08	-	-	-	-	-
C_p for ethanol							
300-590	-731.52567	11.588042	-0.003829199	3.79654E-05	-1.30157E-08	-	-
590-975	17453.966	-32.11887	0.018094754	-	-	-	-
ρ for ethanol							
300-975	-1105.5631	14.724443	-0.038422879	3.79654E-05	-1.30157E-08	-	-
k for ethanol							
300-975	0.16904617	0.000182691	-7.0206E-07	4.86467E-10	-	-	-
μ for ethanol							
300-975	3.96832E-02	-3.61129E-04	1.3689409E-06	-2.7474190E-09	3.0679572E-12	-1.80387E-15	4.35947E-19
C_p for CO_2							
300-363	60207.533	-550.59165	1.720346	-0.001772431	-	-	-
364-1100	14441.085	-66.984943	0.12541195	-0.000102706	3.11002E-08	-	-
ρ for CO_2							
300-1100	5.25032E+03	-2.5521E+01	4.8302009E-02	-4.0461907E-05	1.2545869E-08	-	-
k for CO_2							
300-1100	1.256694	-0.008429452	2.28158E-05	-3.01222E-08	1.9536E-11	-4.9813E-15	-

There was a discrepancy observed in Fluent's calculation of sensible enthalpy (H), which resulted in poor prediction of the C_p spike location in the reactor. Therefore, the UDF for C_p is used to independently calculate enthalpy, using the following equation:

$$H(T) = H(T_1) + C_p(T) * (T - T_{ref}). \quad (8)$$

T_{ref} is set to 27 °C, and T_1 is the lower temperature of the range in which the C_p polynomial fit is valid.

Figure 2 shows the comparison between the NIST database and the polynomial fits for the properties of water along the 25 MPa isobar. The property predictions are well correlated between

the polynomial fit and the NIST database. The polynomial fit predicts the C_p increase at the correct temperature, and the values match the NIST database. Other property curves of k, μ, and ρ are also well predicted by the polynomial fit. Similarly, polynomial fits of ρ and other transport properties are generated for O_2, CO_2, and ethanol.

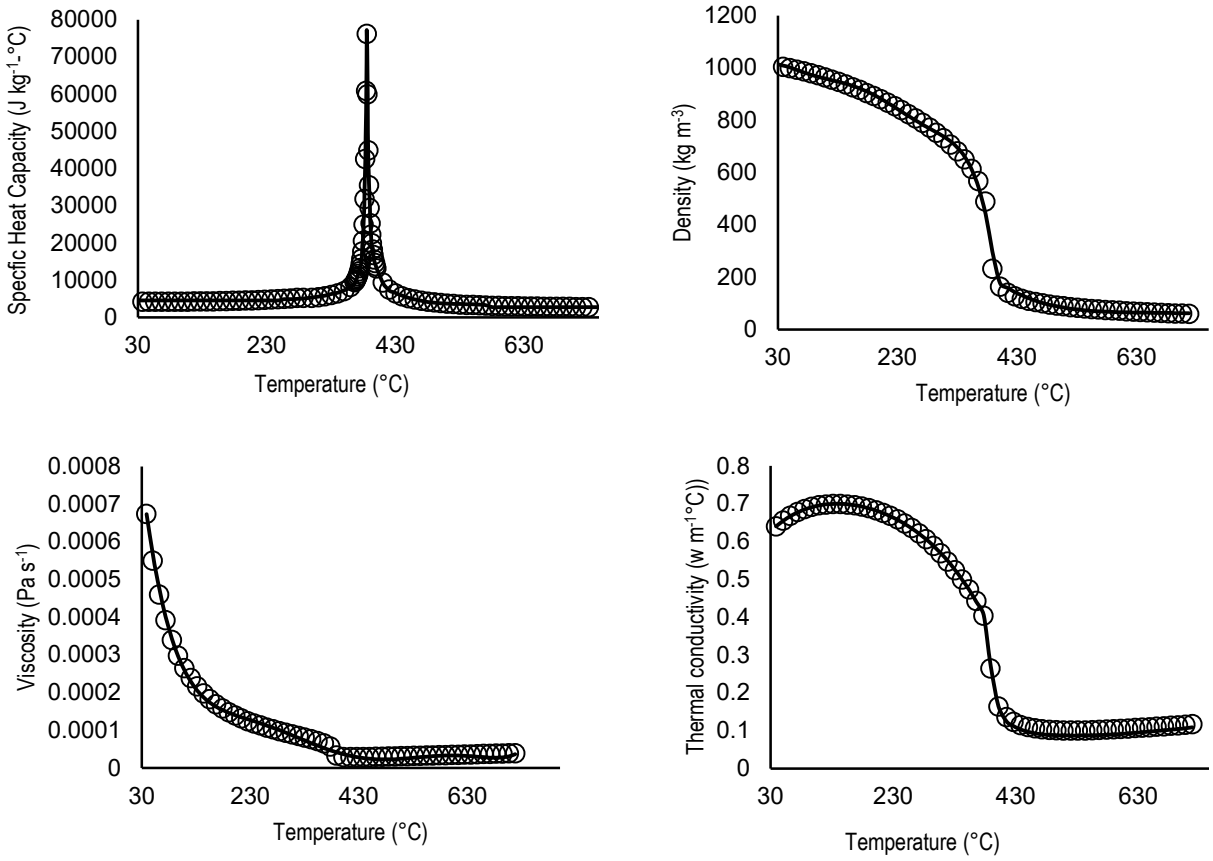

Figure 2. Comparison between the piecewise polynomial functions (—) with the NIST (O) thermophysical properties of water at isobaric conditions (25 MPa).

We evaluated the polynomial fit approach to model non-reacting flow and compared the results against the NIST real gas model[17] available in Fluent 19 software. The limitation of the real gas model cannot be used for reacting flows or mixtures with a molar concentration of water > 5%. We ran two simulations with identical boundary conditions to compare the location of the

transition of SCW to subcritical water in the reactor. The water was preheated to supercritical conditions before entering the reactor. Due to the heat loss, the temperature drops below 374 °C, and a transition to a liquid state occurs. Figure 3(a) compares the drop in temperature in the fluid domain along the reactor length. The polynomial fit model follows the temperature trend of the NIST real gas model. Figure 3(b) compares the C_p CFD profile for the two modeling approaches, predicting the C_p spike at similar positions. This indicates that the polynomial fit is sufficiently accurate for modeling water properties in the reacting flow scenarios.

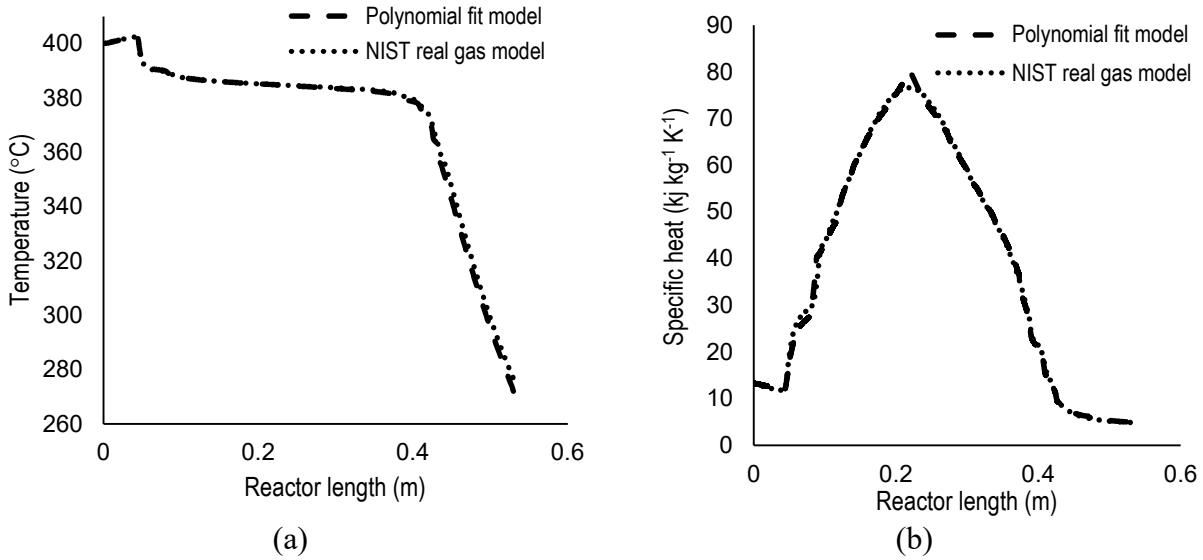

Figure 3. Comparing a) temperature drop and b) C_p prediction between the NIST real gas model and the polynomial fit model. The values are marked on the axis of symmetry of the reactor along its length.

2.4 Validation of the Model with Non-Combustion Experiments

Before running the SCWO simulations, we have used the computational model to simulate the heat loss from the reactor and tuned the material insulating properties. We performed several experiments with only water pumped into the reactor through both the fuel and oxidant lines. Table 3 shows the flow rates and inlet temperatures in these experiments.

Table 3. Inlet boundary condition for the water experiments and as used in the CFD simulations.

Fuel Line (water)		Oxidant line (water)	
Flow Rate (mL min^{-1})	Temperature (°C)	Flow Rate (mL min^{-1})	Temperature (°C)
5.0	400.0	10.0	425.0
5.0	410.0	10.0	440.0
10.0	400.0	10.0	435.0
30.0	382.0	10.0	415.0

The reactor fluid temperature is measured at three locations: 25 mm, 177 mm from the fuel nozzle, and at the reactor exit (380 mm). Thermocouples measuring the temperature of the outer metal wall were also located at the top, middle, and bottom walls of the reactor (Figure 1). Figure 4 shows that the model predicts fluid temperature within 10 °C for all measure locations, including supercritical and subcritical regions. The wall temperatures are also in good agreement with the experiments suggesting that the heat transfer parameters are well-tuned to predict the reactor's heat loss. Based on the non-reacting flow simulations, the polynomial fit approach and the heat transfer model can be used to simulate reacting flow in the SCWO reactor.

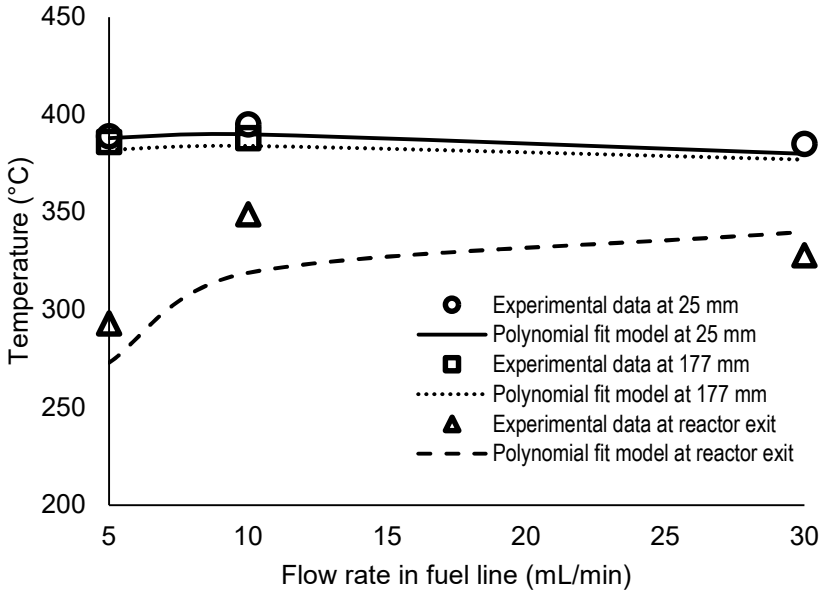

Figure 4. Fluid temperature correlation between water experiments and polynomial fit model. The flow rate of water through the oxidant line is held constant at 10 mL/min, while the flow rate of water through the fuel line is varied and is presented on the x-axis.

2.5 Validation with SCWO Simulation

A series of SCWO experiments were performed to study the oxidation of ethanol.[73] The cases considered in this study are presented in Table 4. The fuel inlet flow is a mixture of ethanol diluted with water. Ethanol flow rate is held constant at 0.86 mL/min for all cases, while the water flow rate varies, changing the molar concentration of ethanol. The global oxidant-fuel equivalence ratio (Φ_{AF}) is defined as:

$$\Phi_{AF} = \frac{\dot{n}_{H_2O_2}/6}{\dot{n}_{ethanol}}, \tag{9}$$

where $\dot{n}_{H_2O_2}$ is the molar flow rate of H_2O_2, and $\dot{n}_{ethan}$ is the molar flow rate of ethanol.

The Φ_{AF} is 1.1 for all cases. The oxidant stream consisting of H_2O_2 diluted with water is injected into the reactor in the coaxial nozzle, see Figure 1. H_2O_2 rapidly decomposes into O_2 and H_2O for the given conditions.[77] To reduce the number of modeled species, our boundary conditions

included only O_2 and H_2O at the ratio consistent with H_2O_2 decomposition. The properties of a multicomponent mixture (ρ, C_p, k, and μ) are calculated as volume-weighted mixing law.

Table 4. Inlet conditions for the combustion experiments and simulations. The total mass flow rate of the oxidant is constant for all the cases.

Fuel Line				Oxidant Line		
Fuel dilution (mol%)	Total mass flow rate (kg s^{-1})	Ethanol mass fraction	T_{in} (°C)	Total mass flow rate (kg s^{-1})	O_2 mass fraction	T_{in} (°C)
2	2.3E-4	0.049	395	1.7E-4	0.15	430
3	1.6E-4	0.073	400			420
4	1.2E-4	0.096	401			411
5	9.7E-5	0.11	401			409
6	8.2E-5	0.14	401			404
7	7.1E-5	0.16	398			401

To model combustion, we use a single step ethanol oxidation mechanism with reaction kinetics proposed by Schanzenbacher et al.[25]

$$C_2H_5OH + 3O_2 \rightarrow 2CO_2 + 3H_2O \quad (10)$$

$$\frac{-\mathrm{d}[C_2H_5OH]}{\mathrm{dt}} = 10^{17.23} \exp\left(\frac{-214\ (\mathrm{kJ}\ mol^{-1})}{\mathrm{RT}}\right) \times [C_2H_5OH]^{1.34}[O_2]^{0.55} \quad (11)$$

The kinetic rates are tested for two combustion models, (i) finite rate, in which the rates are purely controlled by global expression, and (ii) EDC, which models the influence of turbulence on the kinetics. This kinetic modeling approach is not ideal, as the intermediate species participating in the oxidation process are not modeled. Note that in combustion modeling, global rates are often used to avoid significant computational overhead;[78] with the rapid evolution of parallel computing and more efficient numerical codes, the use of the full kinetic mechanism is gaining popularity. However, unlike the gas phase combustion kinetics, the detailed SCWO reaction mechanisms have not been presented in the literature.

3. Model Predictions vs. Experimental Data

3.1 SCWO Experiment vs. Simulation: Kinetic Model Selection

We tested two reaction turbulence-chemistry interaction models: (i) finite rate and (ii) EDC. For a direct comparison, we simulated the 4 mol% ethanol case (see Table 3). The temperature predictions were compared with the experimentally measured fluid and wall temperatures. Table 5 shows that the temperature near the fuel nozzle (~38 mm from the tip) is predicted more accurately by EDC. Both EDC and finite rate predict similar temperatures (within 3 °C) at the midpoint (177 mm from the nozzle). The most significant difference in temperature prediction (103 °C) between the two models is observed in the primary fuel oxidation region, 25 mm from the fuel nozzle. Figure 5 shows that uninhibited by turbulence mixing, the temperature peak predicted by the finite rate model is closer to the nozzle's tip, indicating a faster reaction. The EDC simulations result in a broader primary heat release region and more uniform temperature and species distribution. It appears that EDC predicts temperature better in the most turbulent region (Figure 6), which agrees with the findings of Moussiere et al.[39] Outside of the relatively small region near the fuel jet, the simulations do not show significant differences as the temperature profile is driven by the overall heating value of the fuel stream and the heat loss in the reactor. The authors recognize that the implementation of the detailed chemical kinetic mechanism may change the results as the free radical species or their surrogates (such as CO in a two-step global mechanism) will influence the primary heat release zone.[79] In this work, we used the EDC approach for modeling turbulence-chemistry interaction as it yielded a closer agreement to the experimental data.

Table 5. Temperature correlations between experiments and modeling using finite rate and EDC approaches for the 4 mol% ethanol case.

	25 mm (fluid)	177 mm (fluid)	Reactor exit (fluid)	Top wall	Bottom wall
Exp (°C)	500	467	370	443	372
CFD-FR (°C)	579	439	380	439	423
CFD-EDC (°C)	476	442	384	442	423

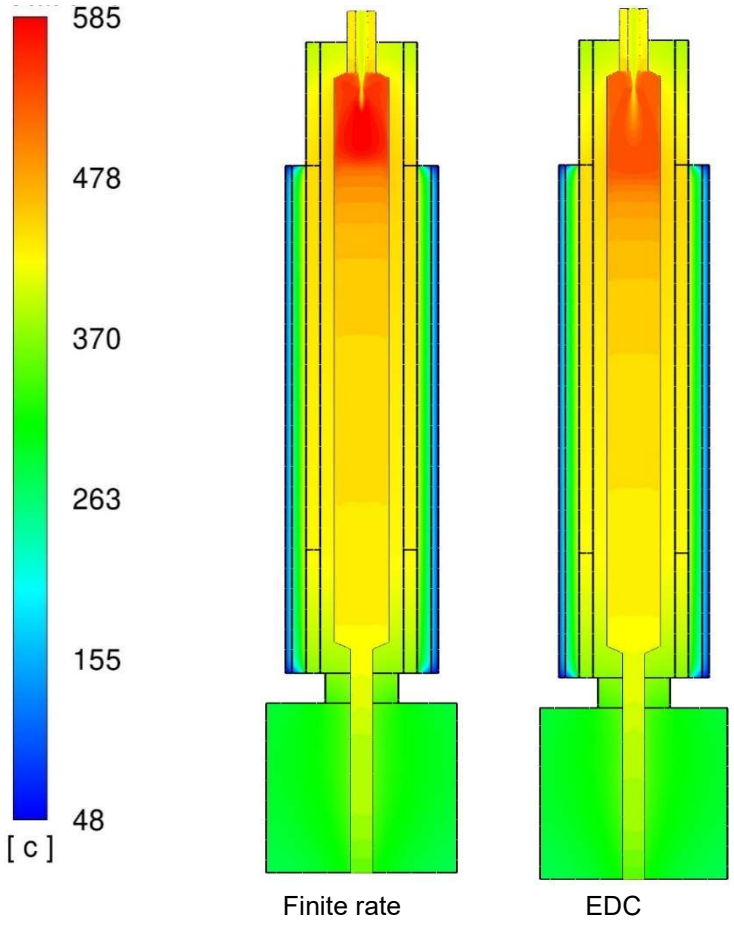

Figure 5. Temperature profiles for 4 mol% ethanol case. The temperature profile by finite rate and EDC model is compared.

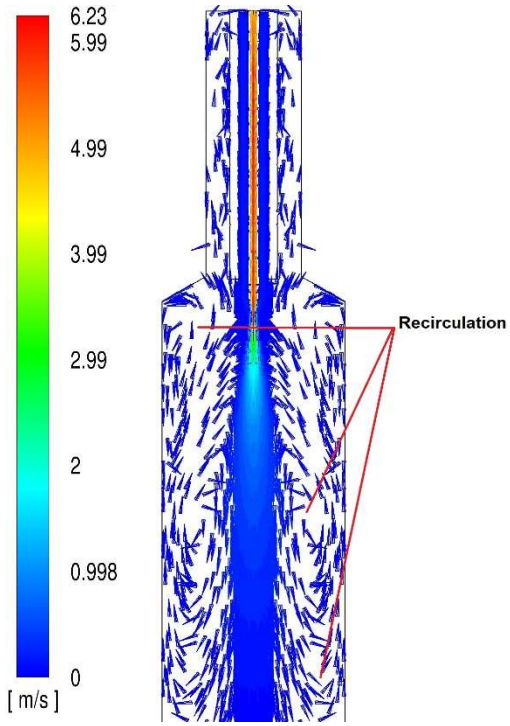

Figure 6. Velocity vectors coloured by velocity showing recirculation zones within 50 mm from the fuel inlet

3.2 Combustion Experiment: Temperature Correlation

Figure 7 compares the temperature profile predictions for the cases with 2, 4, and 7 mol% ethanol concentrations. The data from other cases are included in Table 6. Upon increasing the ethanol concentration, the temperature peak magnitude increases, and the hottest zone in the reactor moves closer to the fuel nozzle. The 7 mol% ethanol case shows high temperature and may be approaching a flaming combustion threshold. These conditions are non-desirable as they may cause reactor damage.

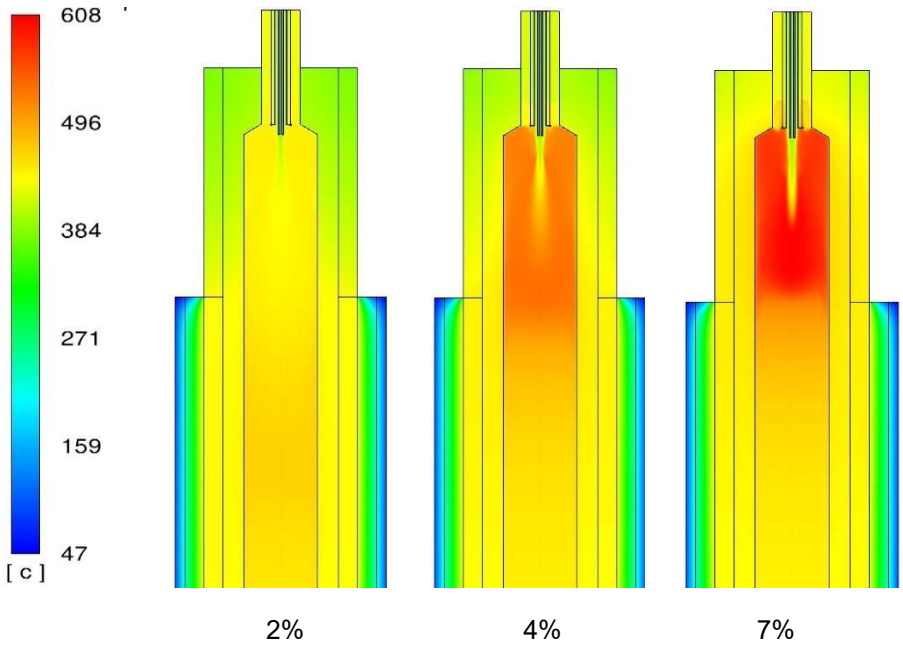

Figure 7. Temperature profiles for ethanol decomposition using the EDC model. The cases compared here are 2, 4, and 7 mol% ethanol.

Figure 8 compares the fluid temperature between the experiments and numerical simulations. The model predicts the jet temperature (25 mm from fuel nozzle tip) within 35 °C of the experimental measurement. The temperature predictions at 177 mm from the fuel nozzle are within 10 to 25 °C, and at the reactor exit, it is within 7 to 15 °C for all cases. The temperature prediction at the wall is within 5% of the experimental value.

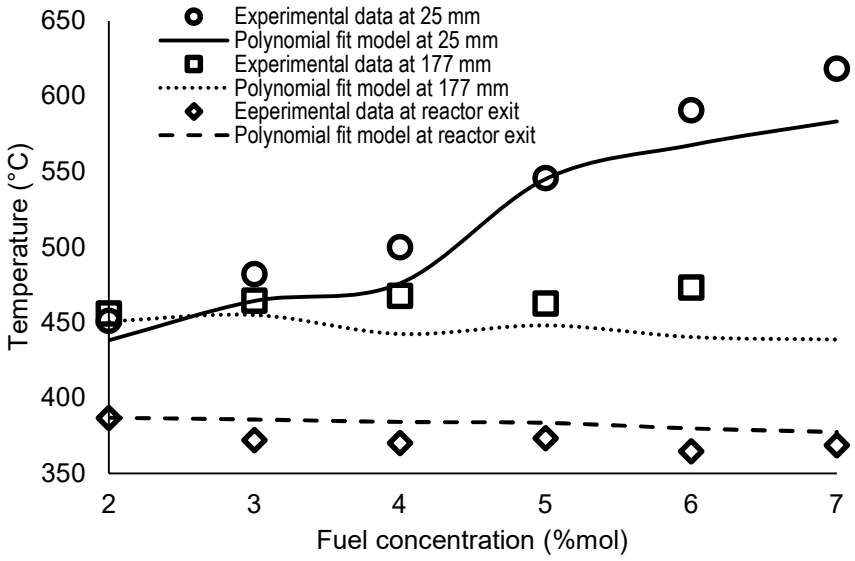

Figure 8. Temperature comparison for ethanol oxidation between the CFD modeling the temperature measurements at 25 mm, 177 mm, and the exit of the reactor.

The profiles for species mass fraction are shown in Figure 9. Complete decomposition of ethanol is observed at all the fuel concentrations. For the 7 mol% case, the ethanol is completely decomposed within 30 mm of the nozzle. The slowest oxidation kinetics are observed for cases low temperatures, i.e., the highest fuel dilution. The species and temperature profiles shed insights into where the fastest reaction rate occurs and whether the transition to liquid water would occur within the reactor cavity. The O_2 spreads more in the reactor top section for the 2 mol% case because of slower reaction kinetics and faster mixing due to higher velocities and turbulence levels.

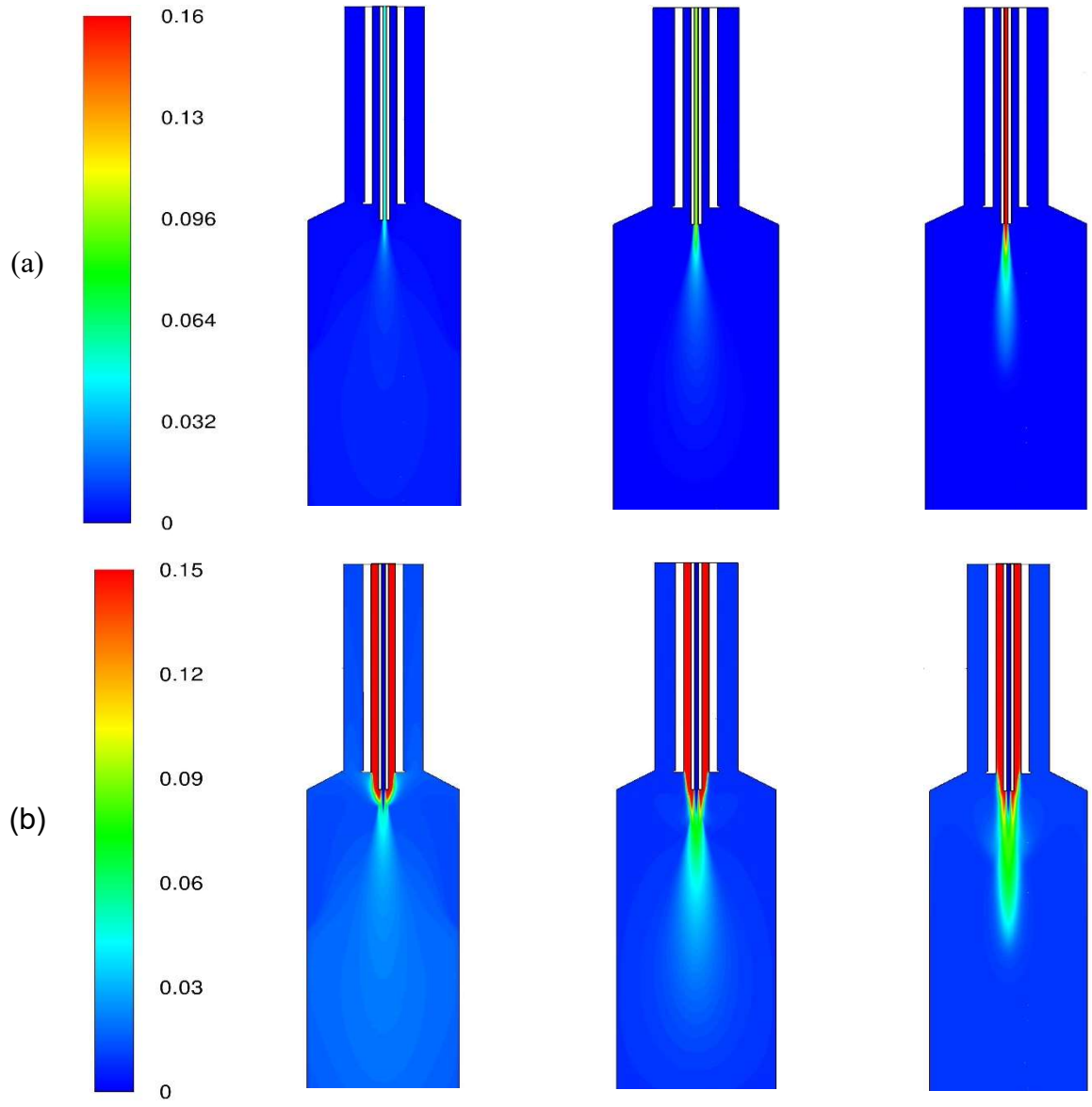
(a)
0.16
0.13
0.096
0.064
0.032
0
(b)
0.15
0.12
0.09
0.06
0.03
0

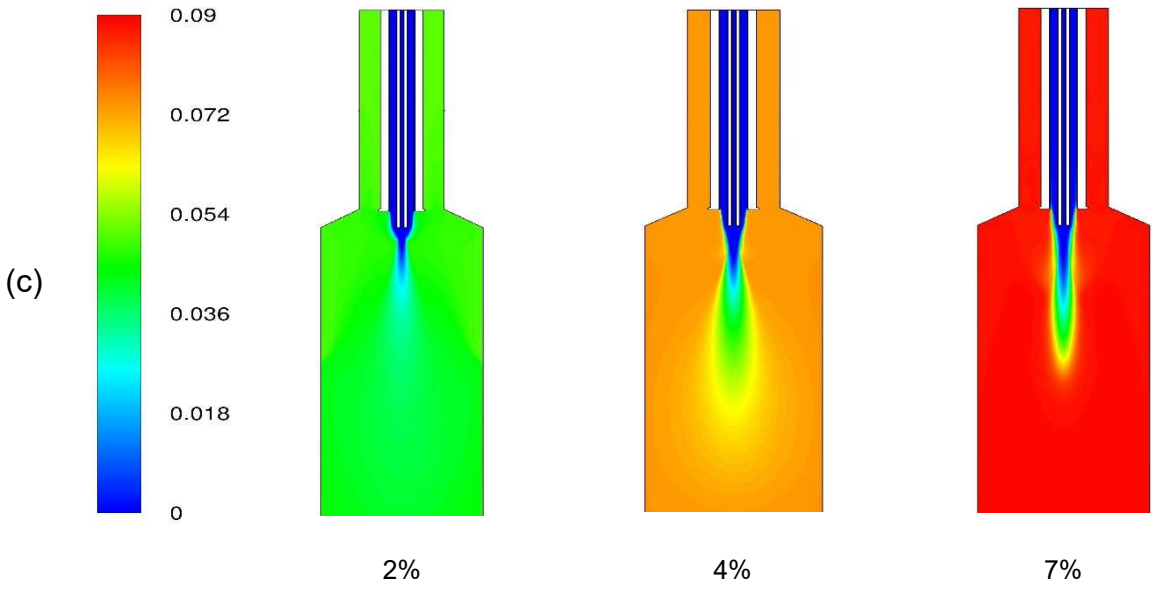

Figure 9. Mass fraction profiles of a) ethanol, b) O_2, and c) CO_2 for 2, 4 and 7 mol% ethanol concentration produced using EDC.

Table 6. Temperature measurements and prediction for both the non-combustion and combustion simulation. In the non-combustion experiments, the flow rate of water from the oxidiser line is held constant at 10mL/min for all cases. For the combustion modeling, EDC kinetic model is used.

	25 mm (fluid)	177 mm (fluid)	Reactor exit (fluid)	Top wall	Bottom wall
Non combustion experiment (fuel flow rate 5 mL/min)					
Exp (°C)	389	386	293	352	330
CFD (°C)	388	378	262	375	368
Non combustion experiment (fuel flow rate 10 mL/min)					
Exp (°C)	395	388	349	362	347
CFD (°C)	390	384	319	378	378
Non combustion experiment (fuel flow rate 30 mL/min)					
Exp (°C)	385	-	328	364	349
CFD (°C)	380	377	340	373	370
Combustion experiment (2 mol% fuel concentration)					
Exp (°C)	451	456	386	404	383
CFD (°C)	438	450	387	437	433
Combustion experiment (3 mol% fuel concentration)					
Exp (°C)	482	464	372	436	373
CFD (°C)	464	455	385.8	450	431
Combustion experiment (4 mol% fuel concentration)					
Exp (°C)	500	467	370	443	372
CFD (°C)	476	442	384	442	423
Combustion experiment (5 mol% fuel concentration)					
Exp (°C)	545	462	373	454	379
CFD (°C)	545	448	383	453	426
Combustion experiment (6 mol% fuel concentration)					
Exp (°C)	590	473	364	464	382
CFD (°C)	567	440	379	451	423

Combustion experiment (7 mol% fuel concentration)					
Exp (°C)	618	-	368	467	349
CFD (°C)	583	438	377	455	422

Damkohler number (*Da*) is the ratio of mixing time to reaction time and is an important parameter to study combustion stability. Low *Da* represents a distributed kinetic regime, where mixing is times are much faster than kinetics. In chemical kinetic modeling, this region is typically represented as PSR. Experimentally in combustion scenarios, it is challenging to achieve the PSR limit even in the high-intensity reactors for hydrocarbon fuels[80-83] and hydrogen.[71, 84] As the combustion approaches the PSR limit, the reaction reaches the blowout. To evaluate the stability of the SCWO process, we examine local *Da* and turbulent *Re* of the location where maximum oxidation rates are observed. The kinetics becomes slow for the 2 mol% case as the ethanol and oxygen spread in the top section of the reactor (Figure 9(a)) as expected in a distributed regime. However, even at these low temperatures, the reactor operated in a stable mode, showing the inherent stability of the inverted gravity SCWO process. Based on the nearly uniform temperature and the species distribution, we show operating in a distributed reaction region possible in the SCWO reactor. This enables predictable exposure to temperature and the oxidative species required to destroy the recalcitrant compounds in a continuous flow reactor. The ability to operate in a distributed regime opens the possibility to model the process using relatively simple chemical reactor networks, i.e., a mix of PSR and PFR elements.[85-87] The reduced-order CRN approach as very efficient and allows to incorporate large chemical kinetic mechanism.

Table 7. Da and turbulent Re number for our boundary conditions near the fuel nozzle. The numbers are compared with Williams' theory and the resultant position of our boundary condition on the regime is estimated.

Fuel mole %	*Da* number	Turbulent *Re* number	Regime position
2	2	10	Distributed regime
4	2	8	Distributed regime

7	30	1.6	Weak turbulence

4. Conclusions

CFD simulation for a small-scale SCWO reactor is presented and validated against measured experimental temperatures. The reactor is represented by a 2D axisymmetric domain. The NSEs are coupled with energy conservation and a single step oxidation chemistry. The heat loss in the reactor is modeled explicitly, including conduction, convection, and radiation mechanisms, to reach a good agreement with the experimental data for fluid and the wall temperatures. The fluid properties are calculated using polynomial fits generated based on the NIST database. The polynomial fit for water properties across the pseudo critical point was validated by comparing it with a real gas model and temperature measurements for non-reacting flow.

In modeling SCWO conditions, the fuel dilution was varied from 2-7% vol of ethanol in water. The chemistry turbulence coupling methods were used: both finite rate and EDC models were found suitable for use in SCWO modeling. The difference between the models was observed near the fuel jet region, where the chemistry is the most active. The EDC was then used to analyze the effect of fuel concentration on temperature values. The fuel temperature prediction in all fuel concentrations was within 30 °C. Analysis of local *Re* and *Da* numbers indicates that the SCWO is stable in a distributed regime due to the excellent stability of the inverted gravity reactor compared to upward flow reactors. Large distributed reaction region suggests that reduced-order modeling of flow field approaches, such as chemical reactor networks, can be developed. Our CFD modeling approach can be used for designing more complex reactors and optimizing the SCWO process.

ASSOCIATED CONTENT

Supporting Information

None.

AUTHOR INFORMATION

Corresponding Author

*ivn@uw.edu; +1 206 543-5248; ORCID: 0000-0002-6347-7450

Author Contributions

The manuscript was written through contributions of all authors. All authors have given approval to the final version of the manuscript.

Funding Sources

Funding for this work was provided by Defense Threat Reduction Agency (DTRA) - Grant HDTRA1-17-1-0001 and a Cooperative Research and Development Agreement (CRADA) with the Army Research Office (ARO) - Project Number CB10397.

ACKNOWLEDGMENTS

Funding for this work was provided by Defense Threat Reduction Agency (DTRA) - Grant HDTRA1-17-1-0001 and a Cooperative Research and Development Agreement (CRADA) with the Army Research Office (ARO) - Project Number CB10397.

NOMENCLATURE

C_p - specific heat [J kg^{-1} K^{-1}]

Da - Damkohler number [-]

E_a - activation energy [kJ mol^{-1}]

g - gravitational constant [m s^{-2}]

H - enthalpy [J/kg]

J - diffusion flux (kg m^{-2} s^{-1})

j_i - specific enthalpy of i^{th} species [J/kg]

k - thermal conductivity [W m^{-1} K^{-1}]

k_{eff} - effective thermal conductivity [W m^{-1} K^{-1}]

$\dot{n}$ - molar flow rate [mol s^{-1}]

p - pressure [Pa]

Re - Reynolds number[-]

S_h - energy source from chemical reaction

S_i - source of i^{th} species from dispersed phase

T - temperature [°C, K]

T_{in} - inlet temperature [°C]

T_{ref} - reference temperature [°C]

u - velocity vector

Y_i - mass fraction of i^{th} species

μ - viscosity [kg/m-s]

ρ - density [kg/m^3]

τ - stress tensor

Φ_{AF} - oxidant-fuel equivalence ratio

ABBREVIATIONS

CFD, Computational fluid dynamics; CRN, chemical reactor network; CWA, chemical warfare agent; DI, deionized; DTRA, Defense Threat Reduction Agency; EDC, eddy dissipation concept; ID, inner diameter; JSR, jet-stirred reactors; LBO, lean blowout; NIST, National Institute of Standards and Technology; NSE, Navier-Stokes equations; PM, particulate matter; PSR, perfectly stirred reactor; RANS, Reynolds-averaged Navier-Stokes; SCW, supercritical water; SCWO, supercritical water oxidation; UDF, user-defined function;

REFERENCES

1. Goto, M.; Nada, T.; Kodama, A.; Hirose, T., Kinetic Analysis for Destruction of Municipal Sewage Sludge and Alcohol Distillery Wastewater by Supercritical Water Oxidation. *Industrial & engineering chemistry research* **1999,** *38* (5), 1863-1865.
2. Svanström, M.; Fröling, M.; Modell, M.; Peters, W. A.; Tester, J., Environmental assessment of supercritical water oxidation of sewage sludge. *Resources, conservation and recycling* **2004,** *41* (4), 321-338.
3. Xu, D.; Wang, S.; Tang, X.; Gong, Y.; Guo, Y.; Wang, Y.; Zhang, J., Design of the first pilot scale plant of China for supercritical water oxidation of sewage sludge. *Chemical engineering research & design* **2012,** *90* (2), 288-297.
4. Baur, S.; Schmidt, H.; Krämer, A.; Gerber, J., The destruction of industrial aqueous waste containing biocides in supercritical water—development of the SUWOX process for the technical application. *The Journal of supercritical fluids* **2005,** *33* (2), 149-157.
5. Bermejo, M. D.; Cocero, M. J., Destruction of an industrial wastewater by supercritical water oxidation in a transpiring wall reactor. *Journal of hazardous materials* **2006,** *137* (2), 965-971.
6. Yang, J.; Wang, S.; Li, Y.; Zhang, Y.; Xu, D., Novel design concept for a commercial-scale plant for supercritical water oxidation of industrial and sewage sludge. *Journal of environmental management* **2019,** *233*, 131-140.
7. Veriansyah, B.; Kim, J.; Lee, J., Destruction of chemical agent simulants in a supercritical water oxidation bench-scale reactor. *Journal of hazardous materials* **2007,** *147* (1-2), 8-14.

8. Bambang Veriansyah Eun-Seok Song Jae-Duck, K., Destruction of methylphosphonic acid in a supercritical water oxidation bench-scale double wall reactor. *Journal of environmental sciences (China)* **2011,** *23* (4), 545-552.
9. Bermejo, M. D.; Rincon, D.; Martin, A.; Cocero, M. J., Experimental Performance and Modeling of a New Cooled-Wall Reactor for the Supercritical Water Oxidation. *Industrial & engineering chemistry research* **2009,** *48* (13), 6262-6272.
10. Mayer, W.; Tamura, H., Propellant injection in a liquid oxygen/gaseous hydrogen rocket engine. *Journal of Propulsion and Power* **1996,** *12* (6), 1137-1147.
11. Oschwald, M.; Smith, J. J.; Branam, R.; Hussong, J.; Schik, A.; Chehroudi, B.; Talley, D., INJECTION OF FLUIDS INTO SUPERCRITICAL ENVIRONMENTS. *Combustion science and technology* **2006,** *178* (1-3), 49-100.
12. Roy, A.; Segal, C., Experimental Study of Fluid Jet Mixing at Supercritical Conditions. *Journal of Propulsion and Power* **2010,** *26* (6), 1205-1211.
13. Kritzer, P., Corrosion in high-temperature and supercritical water and aqueous solutions: a review. *The Journal of Supercritical Fluids* **2004,** *29* (1-2), 1-29.
14. Bermejo, M. D.; Cocero, M. J., Supercritical water oxidation: A technical review. *AIChE journal* **2006,** *52* (11), 3933-3951.
15. Brunner, G., Near and supercritical water. Part II: Oxidative processes. *The Journal of supercritical fluids* **2009,** *47* (3), 382-390.
16. Fauvel, E.; Joussot-Dubien, C.; Tanneur, V.; Moussière, S.; Guichardon, P.; Charbit, G.; Charbit, F., A Porous Reactor for Supercritical Water Oxidation: Experimental Results on Salty Compounds and Corrosive Solvents Oxidation. *Industrial & engineering chemistry research* **2005,** *44* (24), 8968-8971.
17. E.W., L.; I.H., B.; M.L., H.; M.O., M., NIST Standard Reference Database 23: Reference Fluid Thermodynamic and Transport Properties-REFPROP, Version 10.0, National Institute of Standards and Technology, Standard Reference Data Program. Gaithersburg, 2018.
18. Pinkard, B. R.; Gorman, D. J.; Tiwari, K.; Kramlich, J. C.; Reinhall, P. G.; Novosselov, I. V., Review of Gasification of Organic Compounds in Continuous-Flow, Supercritical Water Reactors. *Industrial & Engineering Chemistry Research* **2018,** *57* (10), 3471-3481.
19. Pinkard, B. R.; Gorman, D. J.; Rasmussen, E. G.; Kramlich, J. C.; Reinhall, P. G.; Novosselov, I. V., Kinetics of formic acid decomposition in subcritical and supercritical water – a Raman spectroscopic study. *International Journal of Hydrogen Energy* **2019,** *44* (60), 31745-31756.
20. Pinkard, B. R.; Kramlich, J. C.; Novosselov, I. V., Gasification Pathways and Reaction Mechanisms of Primary Alcohols in Supercritical Water. *ACS Sustainable Chemistry & Engineering* **2020,** *8* (11), 4598-4605.
21. Pinkard, B. R.; Purohit, A. L.; Moore, S. J.; Kramlich, J. C.; Reinhall, P. G.; Novosselov, I. V., Partial Oxidation of Ethanol in Supercritical Water. *Industrial & Engineering Chemistry Research* **2020,** *59* (21), 9900-9911.
22. Savage, P. E., Organic chemical reactions in supercritical water. *Chemical reviews* **1999,** *99* (2), 603-622.
23. Yu, J.; Savage, P. E., Decomposition of formic acid under hydrothermal conditions. *Industrial & Engineering Chemistry Research* **1998,** *37* (1), 2-10.

24. Helling, R. K.; Tester, J. W., Oxidation of simple compounds and mixtures in supercritical water: carbon monoxide, ammonia and ethanol. *Environmental science & technology* **1988,** *22* (11), 1319-1324.
25. Schanzenbächer, J.; Taylor, J. D.; Tester, J. W., Ethanol oxidation and hydrolysis rates in supercritical water. *The Journal of supercritical fluids* **2002,** *22* (2), 139-147.
26. Rice, S. F.; Croiset, E., Oxidation of Simple Alcohols in Supercritical Water III. Formation of Intermediates from Ethanol. *Industrial & engineering chemistry research* **2001,** *40* (1), 86-93.
27. Hayashi, R.; Onishi, M.; Sugiyama, M.; Koda, S.; Oshima, Y., Kinetic analysis on alcohol concentration and mixture effect in supercritical water oxidation of methanol and ethanol by elementary reaction model. *The Journal of supercritical fluids* **2007,** *40* (1), 74-83.
28. Webley, P. A.; Holgate, H. R.; Stevenson, D. M.; Tester, J. W., Oxidation Kinetics of Model Compounds of Metabolic Waste in Supercritical Water. 1990.
29. Brock, E. E.; Oshima, Y.; Savage, P. E.; Barker, J. R., Kinetics and Mechanism of Methanol Oxidation in Supercritical Water. *Journal of physical chemistry (1952)* **1996,** *100* (39), 15834-15842.
30. Anitescu, G.; Zhang, Z.; Tavlarides, L. L., A Kinetic Study of Methanol Oxidation in Supercritical Water. *Industrial & engineering chemistry research* **1999,** *38* (6), 2231-2237.
31. Pinkard, B. R.; Shetty, S.; Kramlich, J. C.; Reinhall, P. G.; Novosselov, I. V., Hydrolysis of Dimethyl Methylphosphonate (DMMP) in Hot-Compressed Water. *The Journal of Physical Chemistry A* **2020,** *124* (41), 8383-8389.
32. Bianchetta, S.; Li, L.; Gloyna, E. F., Supercritical Water Oxidation of Methylphosphonic Acid. *Industrial & engineering chemistry research* **1999,** *38* (8), 2902-2910.
33. Ploeger, J. M.; Green, W. H.; Tester, J. W., Co-oxidation of methylphosphonic acid and ethanol in supercritical water. *The Journal of supercritical fluids* **2006,** *39* (2), 239-245.
34. Zhou, N.; Krishnan, A.; Vogel, F.; Peters, W. A., A computational model for supercritical water oxidation of organic toxic wastes. *Advances in environmental research : an international journal of research in environmental science, engineering and technology* **2000,** *4* (1), 75-90.
35. Narayanan, C.; Frouzakis, C.; Boulouchos, K.; Príkopský, K.; Wellig, B.; Rudolf von Rohr, P., Numerical modelling of a supercritical water oxidation reactor containing a hydrothermal flame. *The Journal of supercritical fluids* **2008,** *46* (2), 149-155.
36. Bermejo, M. D.; Martín, Á.; Queiroz, J. P. S.; Bielsa, I.; Ríos, V.; Cocero, M. J., Computational fluid dynamics simulation of a transpiring wall reactor for supercritical water oxidation. *Chemical engineering journal (Lausanne, Switzerland : 1996)* **2010,** *158* (3), 431-440.
37. Segal, C.; Polikhov, S. A., Subcritical to supercritical mixing. *Physics of Fluids* **2008,** *20* (5), 052101-052101-7.
38. Zhang, F.; Su, C.; Chen, Z.; Chen, J., Experimental study on the mixing characteristics inside an inner preheating transpiring-wall reactor for supercritical water oxidation. *The Journal of supercritical fluids* **2020,** *156*, 104682.
39. Moussière, S.; Joussot-Dubien, C.; Guichardon, P.; Boutin, O.; Turc, H. A.; Roubaud, A.; Fournel, B., Modelling of heat transfer and hydrodynamic with two kinetics approaches during supercritical water oxidation process. *The Journal of supercritical fluids* **2007,** *43* (2), 324-332.
40. Moussiere, S.; Roubaud, A.; Boutin, O.; Guichardon, P.; Fournel, B.; Joussot-Dubien, C., 2D and 3D CFD modelling of a reactive turbulent flow in a double shell supercritical water oxidation reactor. *The Journal of supercritical fluids* **2012,** *65*, 25-31.

41. Huo, H.; Wang, X.; Yang, V., A general study of counterflow diffusion flames at subcritical and supercritical conditions: Oxygen/hydrogen mixtures. *Combustion and flame* **2014,** *161* (12), 3040-3050.
42. Lacaze, G.; Oefelein, J. C., A non-premixed combustion model based on flame structure analysis at supercritical pressures. *Combustion and flame* **2012,** *159* (6), 2087-2103.
43. Abeln, J.; Kluth, M.; Böttcher, M.; Sengpiel, W., Supercritical Water Oxidation (SCWO) Using a Transpiring Wall Reactor: CFD Simulations and Experimental Results of Ethanol Oxidation. *Environmental engineering science* **2004,** *21* (1), 93-99.
44. Dutournié, P.; Mercadier, J.; Matéos, D.; Cansell, F., Hydrothermal oxidation treatment reactor: Experimental and simulated study of a non-anticipated phenomenon at the reactor inlet. *The Journal of supercritical fluids* **2007,** *42* (2), 234-240.
45. Davis, J.; Tiwari, K.; Novosselov, I., Soot morphology and nanostructure in complex flame flow patterns via secondary particle surface growth. *Fuel* **2019,** *245*, 447-457.
46. Liu, P.; Arnold, I. J.; Wang, Y.; Yu, Y.; Fang, J.; Biswas, P.; Chakrabarty, R. K., Synthesis of titanium dioxide aerosol gels in a buoyancy-opposed flame reactor. *Aerosol Science and Technology* **2015,** *49* (12), 1232-1241.
47. Chakrabarty, R. K.; Novosselov, I. V.; Beres, N. D.; Moosmüller, H.; Sorensen, C. M.; Stipe, C. B., Trapping and aerogelation of nanoparticles in negative gravity hydrocarbon flames. *Applied Physics Letters* **2014,** *104* (24), 243103.
48. Mahamuni, G.; Rutherford, J.; Davis, J.; Molnar, E.; Posner, J. D.; Seto, E.; Korshin, G.; Novosselov, I., Excitation–Emission Matrix Spectroscopy for Analysis of Chemical Composition of Combustion Generated Particulate Matter. *Environmental Science & Technology* **2020**.
49. Davis, J.; Molnar, E.; Novosselov, I., Nanostructure transition of young soot aggregates to mature soot aggregates in diluted diffusion flames. *Carbon* **2020,** *159*, 255-265.
50. Hicks, M.; Hegde, U.; Kojima, J., Hydrothermal ethanol flames in Co-flow jets. *The Journal of Supercritical Fluids* **2019,** *145*, 192-200.
51. Kojima, J. J.; Hegde, U. G.; Gotti, D. J.; Hicks, M. C., Flame structure of supercritical ethanol/water combustion in a co-flow air stream characterized by Raman chemical analysis. *The Journal of Supercritical Fluids* **2020,** *166*, 104995.
52. Hodes, M.; Marrone, P. A.; Hong, G. T.; Smith, K. A.; Tester, J. W., Salt precipitation and scale control in supercritical water oxidation—Part A: fundamentals and research. *The Journal of Supercritical Fluids* **2004,** *29* (3), 265-288.
53. Marrone, P. A.; Cantwell, S. D.; Dalton, D. W., SCWO system designs for waste treatment: application to chemical weapons destruction. *Industrial & engineering chemistry research* **2005,** *44* (24), 9030-9039.
54. Serikawa, R. M.; Usui, T.; Nishimura, T.; Sato, H.; Hamada, S.; Sekino, H., Hydrothermal flames in supercritical water oxidation: investigation in a pilot scale continuous reactor. *Fuel* **2002,** *81* (9), 1147-1159.
55. Hazlebeck, D. A.; Downey, K. W.; Spritzer, M. H., Downflow hydrothermal treatment. Google Patents: 2000.
56. Glassman, I.; Yetter, R. A., *Combustion 4th edition*. Academic Press: 2008.
57. Turns, S. R., *An introduction to combustion: concepts and applications, 3rd edition*. McGraw Hill Education: 2012.

58. Radhakrishnan, K.; Heywood, J. B.; Tabaczynski, R. J., Premixed turbulent flame blowoff velocity correlation based on coherent structures in turbulent flows. *Combustion and Flame* **1981,** *42*, 19-33.
59. Karalus, M. F. An investigation of lean blowout of gaseous fuel alternatives to natural gas. 2014.
60. Vijlee, S. Z.; Novosselov, I. V.; Kramlich, J. C. In *Effects of Composition on the Flame Stabilization of Alternative Aviation Fuels in a Toroidal Well Stirred Reactor*, ASME Turbo Expo 2015: Turbine Technical Conference and Exposition, American Society of Mechanical Engineers: 2015; pp V003T03A007-V003T03A007.
61. Vijlee, S. Z.; Kramlich, J. C.; Mescher, A. M.; Stouffer, S. D.; O'Neil-Abels, A. R. In *Characterizing Combustion of Synthetic and Conventional Fuels in a Toroidal Well Stirred Reactor*, ASME Turbo Expo 2013: Turbine Technical Conference and Exposition, American Society of Mechanical Engineers: 2013; pp V01BT04A001-V01BT04A001.
62. Gupta, S.; Malte, P.; Brunton, S. L.; Novosselov, I., Prevention of lean flame blowout using a predictive chemical reactor network control. *Fuel* **2019,** *236*, 583-588.
63. Williams, F. A., *Combustion theory*. CRC Press: 2018.
64. Nanduri, J. R.; Parsons, D. R.; Yilmaz, S. L.; Celik, I. B.; Strakey, P. A., Assessment of RANS-based turbulent combustion models for prediction of emissions from lean premixed combustion of methane. *Combustion Science and Technology* **2010,** *182* (7), 794-821.
65. Magnussen, B. F., On the structure of turbulence and a generalized eddy dissipation concept for chemical reaction in turbulent flow. In *19th American Institute of Aeronautics and Astronautics Aerospace Science Meeting*, St. Louis, Missouri, USA, 1981.
66. Ertesvag, I. S.; Magnussen, B. F., The eddy dissipation turbulence energy cascade model. *Combustion science and Technology* **2000,** *159*, 213-235.
67. Magnussen, B. F., The eddy dissipation concept a bridge between science and technology. In *ECCOMAS Thematic Conference on Computational Combustion*, Lisbon, 2005.
68. Karalus, M. F.; Fackler, K. B.; Novosselov, I. V.; Kramlich, J. C.; Malte, P. C., A skeletal mechanism for the reactive flow simulation of methane combustion. In *ASME Turbo Expo 2013: Turbine Technical Conference and Exposition*, ASME: San Antonio, Texas, USA, 2013; pp 1-10.
69. Karalus, M. F.; Fackler, K. B.; Novosselov, I. V.; Kramlich, J. C.; Malte, P. C., Characterizing the mechanism of lean blowout for a recirculation-stablized premixed hydrogen flame. In *Turbine Technical Conference and Exposition*, ASME Turbo Expo: Copenhagen, Denmark, 2012; pp 21-30.
70. Guan, Y.; Novosselov, I., EVALUATION OF LEAN BLOW-OUT MECHANISM IN TOROIDAL WELL STIRRED REACTOR. *Gas Turbine and Power* **2017,** *Submitted*.
71. Karalus, M. F.; Fackler, K. B.; Novosselov, I. V.; Kramlich, J. C.; Malte, P. C. In *Characterizing the mechanism of lean blowout for a recirculation-stabilized premixed hydrogen flame*, ASME Turbo Expo 2012: Turbine Technical Conference and Exposition, American Society of Mechanical Engineers: 2012; pp 21-30.
72. Guan, Y.; Novosselov, I., Damkohler Number Analysis in Lean Blow-Out of Toroidal Jet Stirred Reactor. *Journal of Engineering for Gas Turbines and Power* **2018,** *140* (10).
73. Moore, S.; Pinkard, B.; Purohit, A.; Misquith, J.; Kramlich, J.; Reinhall, P.; Novosselov, I., Design of a Small-Scale Supercritical Water

Oxidation Reactor. Part I: Experimental Performance and Characterization. ChemRxiv: 2020.

74. Fillingham, P.; Murali, H.; Novosselov, I. V., Nondimensional Parameter for Characterization of Wall Shear Stress From Underexpanded Axisymmetric Impinging Jets. *Journal of Fluids Engineering* **2017,** *139* (11), 111102.
75. Fillingham, P.; Novosselov, I. V., Wall jet similarity of impinging planar underexpanded jets. *International Journal of Heat and Fluid Flow* **2020,** *81*, 108516.
76. Sierra-Pallares, J.; Marchisio, D. L.; Alonso, E.; Parra-Santos, M. T.; Castro, F.; José Cocero, M., Quantification of mixing efficiency in turbulent supercritical water hydrothermal reactors. *Chemical engineering science* **2011,** *66* (8), 1576-1589.
77. Croiset, E.; Rice, S. F.; Hanush, R. G., Hydrogen peroxide decomposition in supercritical water. *AIChE Journal* **1997,** *43* (9), 2343-2352.
78. Novosselov, I. V.; Malte, P. C., Development and application of an eight-step global mechanism for CFD and CRN simulations of lean-premixed combustors. *Journal of Engineering for Gas Turbines and Power* **2008,** *130* (2), 021502.
79. Novosselov, I. V. Eight-Step Global Kinetic Mechanism on Methane Oxidation with Nitric Oxide Formation for Lean-Premixed Combustion Turbines. MSME Thesis, University of Washington, 2002.
80. DePape, P.; Novosselov, I., Model-Based Approach for Combustion Monitoring Using Real-Time Chemical Reactor Network. *Journal of Combustion* **2018,** *2018*.
81. Rutar, T.; Malte, P. C., NOx Formation in High-Pressure Jet-Stirred Reactors with Significance to Lean-Premixed Combustion Turbines. *ASME Journal of Engineering for Gas Turbines and Power* **2002,** *124*, 776-783.
82. Fackler, K. B.; Karalus, M. F.; Novosselov, I. V.; Kramlich, J. C.; Malte, P. C., Experimental and numerical study of NOx formation from the lean premixed combustion of CH4 mixed with CO2 and N2. *Journal of Engineering for Gas Turbines and Power* **2011,** *133* (12), 121502.
83. Fackler, K. B.; Karalus, M.; Novosselov, I.; Kramlich, J.; Malte, P.; Vijlee, S., NOx Behavior for Lean-Premixed Combustion of Alternative Gaseous Fuels. *Journal of Engineering for Gas Turbines and Power* **2016,** *138* (4), 041504.
84. Purohit, A. L.; Nalbandyan, A.; Malte, P. C.; Novosselov, I. V., NNH Mechanism in Low-NOx Hydrogen Combustion:

2 Experimental and Numerical Analysis of Formation Pathways. *Fuel* **2020,** *Submitted*.
85. Novosselov, I. Chemical reactor network modeling of combustion systems. University of Washington Seattle, WA, 2006.
86. Novosselov, I.; Malte, P.; Yuan, S.; Srinivasan, R.; Lee, J. In *Chemical reactor network application to emissions prediction for industial dle gas turbine*, ASME turbo expo 2006: Power for land, sea, and air, American Society of Mechanical Engineers: 2006; pp 221-235.
87. Niksa, S.; Liu, G.-S., Incorporating detailed reaction mechanisms into simulations of coal-nitrogen conversion in pf flames. *Fuel* **2002,** *81* (18), 2371-2385.